Atomistic Study of Lithium Ion Dynamics in $Li_{12}Si_7$

Jianjian Shi,[1] Zhiguo Wang,[1*] Y.Q. Fu[3*]

1 *School of Physical Electronics, University of Electronic Science and Technology of China, Chengdu, 610054, P.R. China*

2 *Department of Physics and Electrical Engineering, Faculty of Engineering and Environment, University of Northumbria, Newcastle upon Tyne, NE1 8ST, UK*

[*]Corresponding author. E-mail: zgwang@uestc.edu.cn (ZW); richard.fu@northumbria.ac.uk (YF)

Abstract

Lithium ion dynamics in crystalline lithium silicide $Li_{12}Si_7$ were studied using density functional theory. Vacancy formation and diffusion of lithium ions showed a strong dependence on crystallographic lithium sites. The thirteen crystallographic lithium atoms in the $Li_{12}Si_7$ can be divided into three types based on their motilities, and their typical diffusion energy barriers are 0.18, 0.36 and 0.52 eV, respectively. These crystallographic lithium atoms take part in the fast diffusion process and distribute within one dimensional column. The result agrees well with experimental report of the quasi-one dimensional fast diffusion channel in the $Li_{12}Si_7$.

Key words: density functional theory, lithium silicide $Li_{12}Si_7$, one dimensional diffusion, fast diffusion

Introduction

Rechargeable lithium ion batteries (LIBs) have received great attention owing to their environmental friendliness, non-memory effect, and high energy density[1]. Graphite has been the dominant anode material for the LIBs with many advantages such as facile synthesis, abundant resources and low volume expansion/contraction of 9%[2]. However, the theoretical capacity of graphite for the LIBs is 372 mA h g^{-1} (LiC_6)[3, 4], which is difficult to meet the strong demands of high energy density and long cycle life for long term applications such as extended range electric vehicles and large scale renewable energy storage. Therefore, the next generation LIBs with a high power density must be implemented using advanced delithiation/lithiation materials as alternative electrode choices.

Group IV elements, such as silicon, germanium, and tin as promising anode materials for the LIBs were extensively investigated by experiments and computational simulation methods[3, 5-8]. Among them, Si was paid considerable attention because of its higher theoretical specific capacity (~3579 mA h g^{-1} for $Li_{15}Si_4$ at room temperature), low cost and abundant resources. However, there is an apparent shortcoming, i.e., Si is easily pulverized upon charging and discharging due to the large volume expansion and shrinkage [3, 4, 9, 10]. Tremendous efforts have been made to overcome this problem using Si nanostructures[11-14], nano-composites of Si with C nanofiber[15-18], Si/Fe multi-layer composites, [19, 20] etc.

It is widely accepted that during the first lithiation cycle, crystalline Si undergoes a phase transition to form an amorphous Li_xSi, but the amorphous Li_xSi alloys can transform into crystalline $Li_{15}Si_4$ when the Li content is x=3.75[9, 21, 22]. The mechanism of the amorphization

process was investigated by Wang et al.[23] using both theoretical analysis and *in-situ* transition electron microscopy observation. They concluded that electron-rich effect plays an important role in the electrochemical solid-state amorphization. Although the thermo-dynamically stable crystalline lithium silicides, i.e., $Li_{12}Si_7$, $Li_{13}Si_4$ and Li_7Si_3 are difficult to observe upon lithiation, they have received considerable interest because they can serve as the reference compounds for the amorphous Li_xSi materials formed upon lithiation. Solid state nuclear magnetic resonance (NMR) studies showed that the amorphous materials have local lithium environments comparable to those present in crystalline silicides, and their quantitative distribution is dependent on the extent of the electrochemical charge transfer, demonstrating their reference capability[24, 25].

A good electrode material should have high electron and Li ion?? mobility and phase stability. The diffusivity value of Li in Si-based electrode materials has been investigated using experimental methods and computer simulations. [26-35] The local environments and dynamics of lithium ions in the binary lithium silicide were studied using NMR technique[36, 37]. Kuhn et al.[37] found that nine of thirteen crystallographically independent Li sites in the $Li_{12}Si_7$ take part in an extreme fast long-range diffusion process characterized by an activation energy of only 0.18 eV in the $Li_{12}Si_7$. In the present paper we studied the Li vacancy formation energies, diffusion energy barriers and Li ion dynamics in the crystalline $Li_{12}Si_7$ alloy using density functional theory. Our results agree well with experimental observations and thus provide an insightful understanding of the mechanism of Li ion dynamics in the $Li_{12}Si_7$ alloy.

Computational details

The crystalline $Li_{12}Si_7$ has an orthorhombic crystal structure. The calculated lattice constants for the $Li_{12}Si_7$ are a=8.646 Å, b=14.576 Å, c=19.989 Å, which are consistent with reported results from other groups[4, 38-40]. There are planar 5Si-rings with Si-Si bond length of 2.362~2.392 Å and a three-pointed planar 4Si star in 'Y'-shape with bond length of 2.375~2.393 Å, as shown in Fig. 1. There are 13 crystallographic lithium sites in the $Li_{12}Si_7$, [37, 39, 40] as represent by balls in different colors in Fig. 1 and their coordinates of Wyckoff sites are listed in Table 1. A supercell with 152 atoms was used in the present work.

The calculations were performed using density functional theory as implemented in the Vienna ab initio package (VASP) [41] with a plane wave basis set. The projector augmented wave (PAW) method[42] was used to describe electron-ion interactions, and the generalized gradient approximation with the Perdew-Burke-Ernzerhof (PBE) function was used to describe the electron exchange-correlation. The K-point mesh for optimization lattice parameters and the calculations of defect formation energies were set to 4×2×2. The plane wave basis-set with a cutoff of 450 eV was used and all atoms were fully relaxed using the conjugate gradient approximation (GGA) until the force on every atom is smaller than 0.02 eV/Å[43, 44]. A climbing image nudged elastic band (CI-NEB)[45] method was used to study the energy curves for Li ions from one stable site to a neighboring stable one.

The formation energy of Li vacancy in the $Li_{12}Si_7$ alloy $E_f(\mathrm{Vac_{Li}})$ was calculated using the equation (1):

$$E_f(\mathrm{Vac_{Li}}) = E(\mathrm{Vac_{Li}}) - E(\mathrm{perf}) + \mu(\mathrm{Li}) \quad (1)$$

where $E(\mathrm{Vac_{Li}})$ and E(perf) are the total energies of the same $Li_{12}Si_7$ supercell with and without a lithium atom vacancy, respectively. μ(Li) is the chemical potential of the bulk Li [46-48].

Ab initio molecular dynamics (MD) simulations were performed within the framework of DFT as implemented Spanish Initiative for Electronic with Thousands of Atoms (SIESTA) code[49-52]. All calculations were performed using the 152 atoms supercell with one Li vacancy. The valence electron wave functions were expanded using a double-ζ basis set. The charge density was projected on a real space grid with a cut-off of 150 Ry to calculate the self-consistent Hamiltonian matrix elements, and Γ point was used in the Brillouin zone sampling. The evolution of the system was derived using the MD method with a verlet algorithm and a time-step of 1.0 fs. The time of 6 ps was verified to be sufficient for the observation of Li in the $Li_{12}Si_7$. Temperatures of 900 K, 1000K and 1100K were applied during the simulation under the NVT ensemble, in which number of atoms, volume and temperature were kept as constant values.

Results and discussions

The vacancy formation energies of 13 crystallographic Li atoms in the $Li_{12}Si_7$ are shown in Fig. 2(a). The vacancies for Li3, Li6 and Li13 have high formation energies of 1.28, 1.34 and 1.23 eV, respectively. Those of Li2 and Li4 have middle formation energies of 1.01 and 1.02 eV, respectively. Whereas those of the Li1, Li5, Li7-12 have low formation energies in the range between 0.74 and 0.92 eV. High formation energies of Li vacancy generally indicate that

Li ions in these sites are immobile, whereas the low formation energy values mean that these Li ions can migrate easily. The vacancy formation energies of the crystallographic Li sites (apart from?? ~~except for~~ the Li13 site) agree with the experimental results obtained by Kuhn et al.[37] The site dependence of the vacancy formation energy can be explained by the differences in the local atomic environments (as shown in Fig. 2 (b)): (1) Li3 is bound to two 5Si-rings with 4 Li-Si bonds and one 4Si star with one Li-Si bond, and Li6 is sandwiched between two 5Si rings and bound tightly to 5Si-ring with 10 Li-Si bonds. Therefore, Li3 and Li6 are tightly bound to the Zintl anions in the structure, thus having large vacancy formation energies; (2) Li2 and Li4 ions are bound to three 5Si-ring with 5 Li-Si bonds; (3) Li12 and Li13 ions are bound to both two 5Si-ring with 2 Li-Si bonds and one 4Si star with one and three Li-Si bonds, respectively; (4) other Li ions are weakly bound to the Si atoms, so they are mobile with low vacancy formation energies.

We calculated several Li ion diffusion paths in the $Li_{12}Si_7$ through Li vacancy migration. The diffusion energy curves are shown in Fig. 3 (a), and the corresponding diffusion paths are shown in Fig. 3 (b). Based on Fig. 3 (a), the diffusion barriers for the Li ions migrating from Li6 to Li5, and from L6 to Li4 are 0.52 and 0.38 eV, respectively. The data agree well with the experimental value of 0.55 eV[37]. The diffusion barrier values for the Li ions migrating from Li4 to Li10, and from Li4 to Li11 are 0.36 and 0.19 eV, respectively, which agrees with experimental value of 0.32 eV[37]. The diffusion barrier value is 0.06 eV for a Li ion migrating from Li5 to Li11. The diffusion barriers are in agreement with the jump barrier values reported by Kuhn et al.[37] The ionic mobility barriers are closely correlated with the calculated vacancy

formation energies. A high vacancy formation energy corresponds to a large diffusion barrier. For example, the vacancy formation energy is 1.34 eV for the Li6 ion, but diffusion barriers of 0.38 and 0.52 eV have to be overcome when the Li6 ion jumps to Li4 and Li5 sites, respectively.

MD simulation was performed at 900 K-1100 K for the $Li_{12}Si_7$ with one Li6 vacancy. Fig. 4 (a) shows the sequence of Li ion migrations at 900 K, with the number denoting the different Li atoms and the number Lix in the brackets denoting the distinct crystallographic lithium. The typical atom displacement distances as a function of simulation time are shown in Fig 4 (b) and their migration trajectories are shown in Fig. 4 (c). As expected one 40(Li2) atom moves to the Li6 vacancy at about 0.2 ps, and thus leaves a vacancy at 40(Li2) site. The Li atom of number 40(Li2) does not involve in the diffusion process at the later simulation process. The Li atom of 74(Li7) migrates to the 40(Li2) vacancy site at about 0.6 ps. The Li diffusion proceeds with more vacancies moving further. At 5.5 ps, the Li atom of 8 (Li13) jumps to a Li11 vacancy. It can be seen from Fig. 4 (a) that both Li3 and Li6 have not taken part in diffusion within the simulation time of 6.0 ps in the $Li_{12}Si_7$. The atom of 8(Li13) involves in the diffusion process, however, it remains in its original position for much longer time than the others during the diffusion. Results also show that migration of the Li3 and Li6 atoms at 1000 and 1100 K did not occur within the simulation time. The Li2, Li4 and Li13 atoms are involved in the diffusion process once for all the simulated temperatures. Atoms of the Li1, Li5, Li17-Li12 are actively involved in the diffusion process. Results indicate that Li atoms with low vacancy formation

energies actively take part in a fast Li diffusion process, which agree with the above calculated results of vacancy formation energies and diffusion barriers.

From the above results, it can be concluded that the 13 distinct crystallographic lithium atoms can be divided into three types: i.e., (1) Li1, Li5, Li7-Li12 atoms, which show fast diffusion process; (2) Li3 and Li6 atoms, which have a low mobility and bounded to the silicon; (3) Li2, Li4 and Li13 atoms, which have medium mobility. The Li atoms with fast, medium and low diffusion mobilities are shown in Fig. 5 with green, pink and red balls, respectively. It can be observed that the fast diffusion Li atoms are distributed within one dimensional column, which agrees well with the quasi-one dimensional diffusion channels observed by Kuhn et al.[27] using the NMR technique.

Conclusions

The Li ion dynamics in crystalline lithium silicide $Li_{12}Si_7$ were investigated using density functional theory. The vacancy formation and diffusion of lithium ion show strong dependence on crystallographic lithium sites. The thirteen crystallographic lithium atoms can be divided into three types with high, medium, and low motilities, and their typical diffusion barriers are 0.18, 0.36 and 0.52 eV, respectively. Eight of thirteen Li sites take part in the fast diffusion process, and are distributed within one dimensional column, showing a fast one dimensional diffusion channel. Large vacancy formation energies are corresponding to the large diffusion barriers and low probability to migrate.

Acknowledgement:

This work was financially supported by the National Natural Science Foundation of China (11474047). Funding support from Royal academy of Engineering UK-Research Exchange with China and India is acknowledged.

References:

1. Bandhauer, T. M.; Garimella, S.; Fuller, T. F. *Journal of the Electrochemical Society* **2011,** 158, (3), R1-R25.
2. Kambe, N.; Dresselhaus, M. S.; Dresselhaus, G.; Basu, S.; McGhie, A. R.; Fischer, J. E. *Materials Science and Engineering* **1979,** 40, (1), 1-4.
3. Chou, C.-Y.; Kim, H.; Hwang, G. S. *The Journal of Physical Chemistry C* **2011,** 115, (40), 20018-20026.
4. Kim, H.; Chou, C.-Y.; Ekerdt, J. G.; Hwang, G. S. *The Journal of Physical Chemistry C* **2011,** 115, (5), 2514-2521.
5. Jung, H.; Allan, P. K.; Hu, Y. Y.; Borkiewicz, O. J.; Wang, X. L.; Han, W. Q.; Du, L. S.; Pickard, C. J.; Chupas, P. J.; Chapman, K. W.; Morris, A. J.; Grey, C. P. *Chemistry of Materials* **2015,** 27, (3), 1031-1041.
6. Lim, L. Y.; Liu, N.; Cui, Y.; Toney, M. F. *Chemistry of Materials* **2014,** 26, (12), 3739-3746.
7. Wu, X. L.; Guo, Y. G.; Wan, L. J. *Chem-Asian J* **2013,** 8, (9), 1948-1958.
8. Nithyadharseni, P.; Reddy, M. V.; Nalini, B.; Kalpana, M.; Chowdari, B. V. R. *Electrochimica Acta* **2015,** 161, 261-268.
9. Xu, Y. H.; Yin, G. P.; Zuo, P. J. *Electrochimica Acta* **2008,** 54, (2), 341-345.
10. Liu, X. H.; Wang, J. W.; Huang, S.; Fan, F.; Huang, X.; Liu, Y.; Krylyuk, S.; Yoo, J.; Dayeh, S. A.; Davydov, A. V.; Mao, S. X.; Picraux, S. T.; Zhang, S.; Li, J.; Zhu, T.; Huang, J. Y. *Nat Nanotechnol* **2012,** 7, (11), 749-56.
11. Wu, H.; Cui, Y. *Nano Today* **2012,** 7, (5), 414-429.
12. Zhang, F.; Yang, X.; Xie, Y. Q.; Yi, N. B.; Huang, Y.; Chen, Y. S. *Carbon* **2015,** 82, 161-167.
13. Hwa, Y.; Kim, W. S.; Yu, B. C.; Kim, J. H.; Hong, S. H.; Sohn, H. J. *Journal of Power Sources* **2014,** 252, 144-149.
14. Nienhaus, H.; Karacuban, H.; Krix, D.; Becker, F.; Hagemann, U.; Steeger, D.; Bywalez, R.; Schulz, C.; Wiggers, H. *Journal of Applied Physics* **2013,** 114, (3), 034310.
15. Tian, H.; Tan, X.; Xin, F.; Wang, C.; Han, W. *Nano Energy* **2015,** 11, 490-499.
16. Chang, X. H.; Li, W.; Yang, J. F.; Xu, L.; Zheng, J.; Li, X. G. *J Mater Chem A* **2015,** 3, (7), 3522-3528.
17. Li, S. L.; Chen, C.; Fu, K.; Xue, L. G.; Zhao, C. X.; Zhang, S.; Hu, Y.; Zhou, L.; Zhang, X. W. *Solid State Ionics* **2014,** 254, 17-26.
18. Ji, L. W.; Zhang, X. W. *Energ Environ Sci* **2010,** 3, (1), 124-129.
19. Kang, H. K.; Lee, S. R.; Cho, W. I.; Cho, B. W. *Physical Chemistry Chemical Physics* **2013,** 15, (5), 1569-1577.
20. Kim, J. B.; Jun, B. S.; Lee, S. M. *Electrochimica Acta* **2005,** 50, (16-17), 3390-3394.
21. Meng Gu, Z. W., Justin G.connell, Daniel E. Perea, Lincoln J. Lauhon, Fei Gao, and Chongmin wang. *ACS Nano* **2013,** 7, (7), 6303-6309.

22. Wang, C. M.; Li, X.; Wang, Z.; Xu, W.; Liu, J.; Gao, F.; Kovarik, L.; Zhang, J. G.; Howe, J.; Burton, D. J.; Liu, Z.; Xiao, X.; Thevuthasan, S.; Baer, D. R. *Nano letters* **2012,** 12, (3), 1624-32.
23. Wang, Z.; Gu, M.; Zhou, Y.; Zu, X.; Connell, J. G.; Xiao, J.; Perea, D.; Lauhon, L. J.; Bang, J.; Zhang, S.; Wang, C.; Gao, F. *Nano letters* **2013,** 13, (9), 4511-6.
24. Key, B.; Bhattacharyya, R.; Morcrette, M.; Seznec, V.; Tarascon, J. M.; Grey, C. P. *Journal of the American Chemical Society* **2009,** 131, (26), 9239-9249.
25. Key, B.; Morcrette, M.; Tarascon, J. M.; Grey, C. P. *Journal of the American Chemical Society* **2011,** 133, (3), 503-512.
26. Yoshimura, K.; Suzuki, J.; Sekine, K.; Takamura, T. *Journal of Power Sources* **2007,** 174, (2), 653-657.
27. Kuhn, A.; Sreeraj, P.; Poettgen, R.; Wiemhoefer, H.-D.; Wilkening, M.; Heitjans, P. *Journal Of the American Chemical Society* **2011,** 133, (29), 11018-11021.
28. Wan, W.; Zhang, Q.; Cui, Y.; Wang, E. *Journal Of Physics-Condensed Matter* **2010,** 22, (41).
29. Zhang, Q.; Zhang, W.; Wan, W.; Cui, Y.; Wang, E. *Nano Letters* **2010,** 10, (9), 3243-3249.
30. Zhang, Q.; Cui, Y.; Wang, E. *Journal Of Physical Chemistry C* **2011,** 115, (19), 9376-9381.
31. Tritsaris, G. A.; Zhao, K. J.; Okeke, O. U.; Kaxiras, E. *Journal Of Physical Chemistry C* **2012,** 116, (42), 22212-22216.
32. Jung, S. C.; Han, Y.-K. *Physical Chemistry Chemical Physics* **2011,** 13, (48), 21282-21287.
33. Malyi, O. I.; Tan, T. L.; Manzhos, S. *Applied Physics Express* **2013,** 6, (2).
34. Wang, Z.; Su, Q.; Deng, H.; He, W.; Lin, J.; Fu, Y. Q. *Journal Of Materials Chemistry A* **2014,** 2, (34), 13976-13982.
35. Johari, P.; Qi, Y.; Shenoy, V. B. *Nano Letters* **2011,** 11, (12), 5494-5500.
36. Dupke, S.; Langer, T.; Winter, F.; Pottgen, R.; Winter, M.; Eckert, H. *Solid State Nucl Magn Reson* **2015,** 65, 99-106.
37. Kuhn, A.; Dupke, S.; Kunze, M.; Puravankara, S.; Langer, T.; Pottgen, R.; Winter, M.; Wiemhofer, H. D.; Eckert, H.; Heitjans, P. *J Phys Chem C* **2014,** 118, (49), 28350-28360.
38. Dupke, S.; Langer, T.; Pottgen, R.; Winter, M.; Eckert, H. *Solid State Nucl Magn Reson* **2012,** 42, 17-25.
39. Nesper, R.; von Schnering, H. G.; Curda, J. *Chemische Berichte* **1986,** 119, (12), 3576-3590.
40. von Schnering, H. G.; Nesper, R.; Curda, J.; Tebbe, K. F. *Angewandte Chemie International Edition in English* **1980,** 19, (12), 1033-1034.
41. Kresse, G.; Furthmuller, J. *Computational Materials Science* **1996,** 6, (1), 15-50.
42. Kresse, G.; Joubert, D. *Phys. Rev. B* **1999,** 59, (3), 1758-1775.
43. Hoang, K.; Johannes, M. *Chemistry of Materials* **2011,** 23, (11), 3003-3013.
44. López-Corral, I.; de Celis, J.; Juan, A.; Irigoyen, B. *Int J Hydrogen Energ* **2012,** 37, (13), 10156-10164.
45. Henkelman, G.; Uberuaga, B. P.; Jo´nsson, H. *J Chem Phys* **2000,** 113, (22), 9901-9904.
46. Wei, S.-H.; Zhang, S. B. *Phys Rev B* **2002,** 66, (15).
47. Wei, S.-H.; Zhang, S. B.; Zunger, A. *Journal of Applied Physics* **2000,** 87, (3), 1304.
48. Duan, H.; Li, J.; Chiang, S. W.; Du, H.; Duan, W. *Comp Mater Sci* **2015,** 96, 263-267.
49. Bujakiewicz-Koronska, R.; Nalecz, D. M. *Phase Transit* **2013,** 86, (2-3), 167-174.
50. Sanchez-Portal, D.; Ordejon, P.; Canadell, E. *Struct Bond* **2004,** 113, 103-170.
51. Montejano-Carrizales, J. M.; Aguilera-Granja, F.; Goyhenex, C.; Pierron-Bohnes, V.; Morán-López, J. L. *J Magn Magn Mater* **2014,** 355, 215-224.
52. Yao, Y. S.; Martonak, R.; Patchkovskii, S.; Klug, D. D. *Phys Rev B* **2010,** 82, (9).

Table 1: Optimized coordinates of 13 crystallographic lithium Wyckoff sites in the $Li_{12}Si_7$

#	Wyckoff site	x	y	z
1	8d	0.1229	0.3404	0.1657
2	8d	0.6296	0.0657	0.9722
3	8d	0.3696	0.7365	0.1127
4	8d	0.6331	0.4327	0.9952
5	8d	0.6282	0.3612	0.1451
6	8d	0.1295	0.2563	0.0316
7	8d	0.8621	0.5222	0.3286
8	8d	0.1375	0.8374	0.3119
9	8d	0.3913	0.1567	0.8128
10	8d	0.1576	0.5050	0.1117
11	8d	0.5037	0.5276	0.1250
12	4c	0.3382	0.1658	0.2500
13	4c	0.3869	0.3687	0.2500

Figure captions:

Figure 1 Crystal structure of $Li_{12}Si_7$. 13 distinct crystallographic lithium atoms are present in different colors. The big blue ball represents Si atom.

Figure 2 (a) Li vacancy formation energies histograms and (b) local atomic environments structure of 13 distinct crystallographic Li atoms in the $Li_{12}Si_7$.

Figure 3 (a) The diffusion energy barrier curves for the Li diffusion Li10→Li4→Li11 →Li5→Li6→Li4. (b) The diffusion paths of Li10→Li4, Li4→Li11, Li11→Li5, Li5→Li6, and Li6→Li4.

Figure 4 (a) The Li ion migration sequence in the $Li_{12}Si_7$ started with one Li6 vacancy at 900K. The number denotes the different Li atoms, the number Lix in the brackets denotes the distinct crystallographic lithium. (b) Typical atom displacement distances as a function of simulation time. (c) Trajectories of the Li atoms in (b).

Figure 5 Diagrammatic sketches of three different lithium diffusion types. The fast, medium, and low Li diffusion atoms are represented by green, pink and red balls, respectively. The regions surrounded by green dotted line denote one dimension channel of fast Li diffusion.

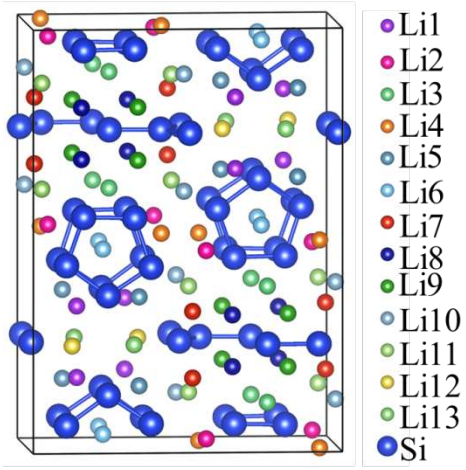

J.J. Shi et al. Figure 1

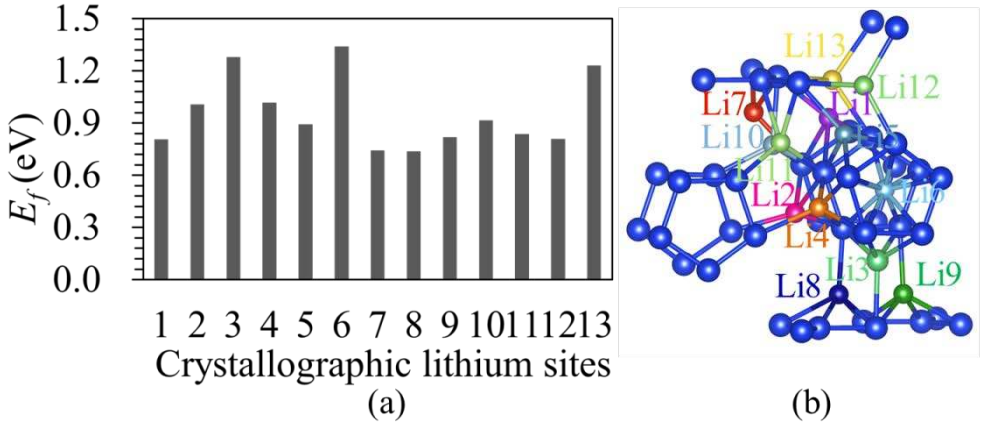

J.J. Shi et al. Figure 2

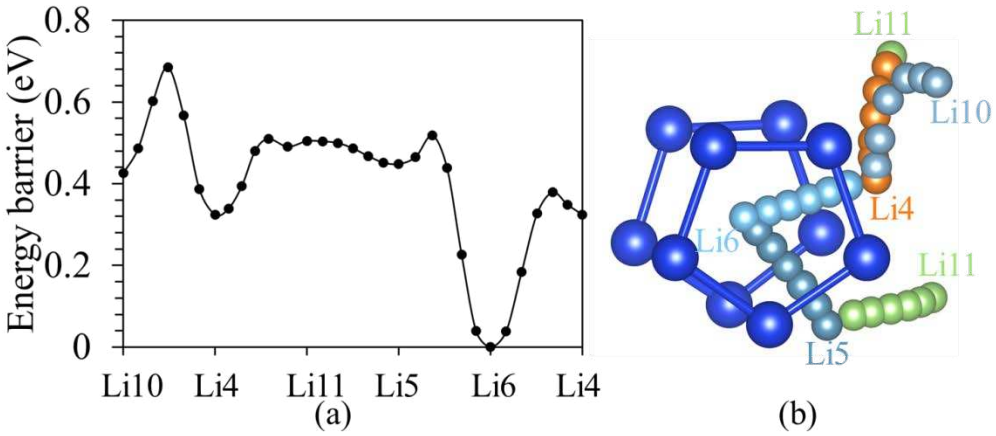

J.J. Shi et al. Figure 3

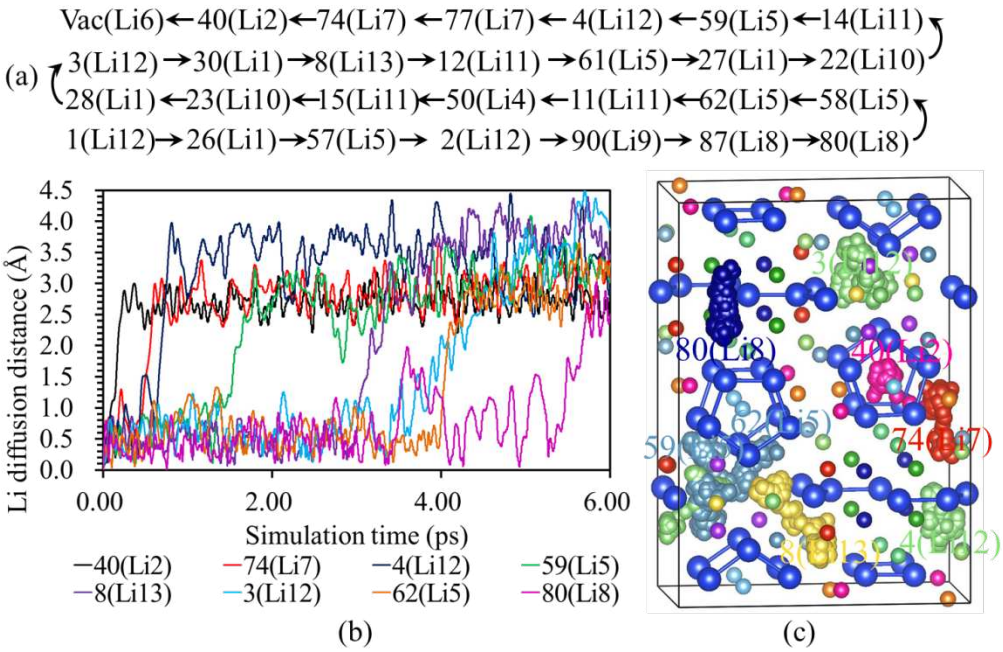

J.J. Shi et al. Figure 4

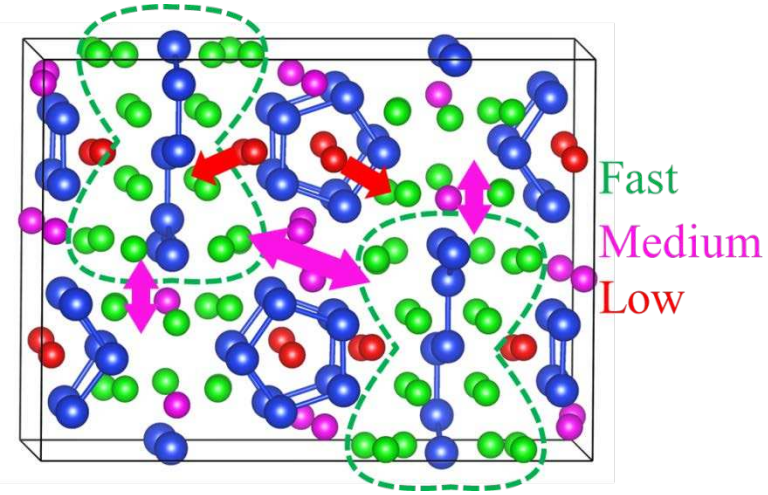

J.J. Shi et al. Figure 5